

Acoustic wave propagation and scattering for fault detection in composite honeycomb panels

V. Hafiychuk V. Smelyanskiy D. Timuçin S. Schuet
K. Wheeler R. Tyson J. Walker

12 September 2013

ABSTRACT

This paper reports on an effort to develop and demonstrate structural health monitoring—specifically, fault detection and localization—algorithms for composite sandwich panels. The test artifact was a small panel consisting of an aluminum honeycomb core sandwiched between two carbon-fiber face sheets, and featuring a controlled impact damage on one side. Data were collected on the damaged side of the panel using a network of piezo-electric sensors mounted on the face sheet. Two (potentially complementary) algorithms were implemented for detecting and localizing the fault from ultrasound data collected before and after damage. The algorithms use variants of the standard least-squares approach for estimating damage location, and are distinguished mainly by their reliance on qualitative versus quantitative physics models of acoustic wave propagation in the panel. Successful detection and localization of a sub-inch fault is demonstrated.

INTRODUCTION

Composite sandwich panels are light-weight structural elements that offer high performance (high strength, damage tolerance, and thermal resistance) with flexible production capabilities [1, 2]. During the past few decades, these types of elements have been steadily replacing traditional materials in aerospace applications. Their stiffness-to-weight ratios and damage tolerance are especially attractive in space vehicle designs (e.g., NASA’s new heavy-lift launch vehicle) as they enable heavier payloads.

The goal of the present study was to develop a theoretically sound and experimentally validated approach for structural health monitoring (SHM), and specifically fault detection and localization, in a type of composite sandwich

V. Hafiychuk, V. Smelyanskiy, D. Timuçin, S. Schuet, and K. Wheeler are with NASA Ames Research Center, Moffett Field, CA 94035, USA.

J. Walker is with NASA Marshall Space Flight Center, Huntsville, AL 35812, USA.

R. Tyson is with University of Alabama, 1804 Sparkman Dr., Huntsville, AL 35816, USA.

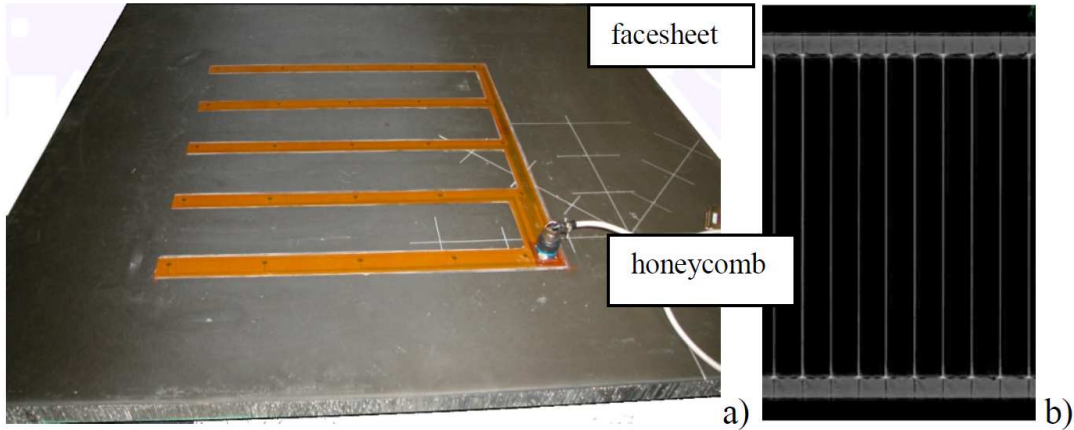


Figure 1: General view of the $4' \times 4'$ test panel with Acellent SMART Layer[®] mounted on one side (a), and CT scan (side view) of the panel structure (b).

panel being considered for space applications. For this purpose, a representative test panel was constructed and instrumented with an array of piezo-electric sensors that can excite and detect acoustic waves on the panel. The anti-symmetric Lamb wave (A_0) was expected to be the dominant mode, given the typical thickness of composite structures being considered. Relatively low attenuation of the A_0 mode and the high efficiency and sensitivity of low-cost piezoelectric actuators suggest an effective method for SHM of composite sandwich panels.

EXPERIMENTAL SETUP

A $4' \times 4'$ test panel was fabricated for this study (see Fig. 1) by bonding two 16-layer cross-ply carbon-fiber laminate face sheets to a 1.5"-thick aluminum honeycomb core. The panel was instrumented with a SMART Layer[®] [3], courtesy of Acellent Technologies, Inc., which consisted of a 5×5 PZT sensor grid with a pitch of about 5.4" (Fig. 1a).

The SMART Layer[®] allowed for the excitation of Lamb waves by driving any one of the actuators with a voltage signal $v(t)$ while listening on the remaining 24 sensors. (During experiments, the panel was placed vertically, and the bottom edge was isolated from the laboratory floor by soft foam.) A commonly used narrowband input voltage waveform is the Hann signal

$$v(t) = \frac{A}{2} \sin(\omega_0 t) \left[1 - \cos\left(\frac{2\pi t}{T}\right) \right] [s(t) - s(t - T)], \quad (1)$$

where A , T , and ω_0 respectively denote the amplitude, the duration, and the center frequency of the wave packet, and $s(\cdot)$ is the Heaviside step function. The driving frequency $f_0 = \omega_0/2\pi$ was chosen in the range 20 to 180 kHz, which was critical for the proper excitation of Lamb waves on the panel.

The panel was subsequently subjected to controlled impacts by a semi-spherical impactor with a head diameter of about 0.5". Based on earlier calibration tests using a similar panel, the impact energy was adjusted to produce

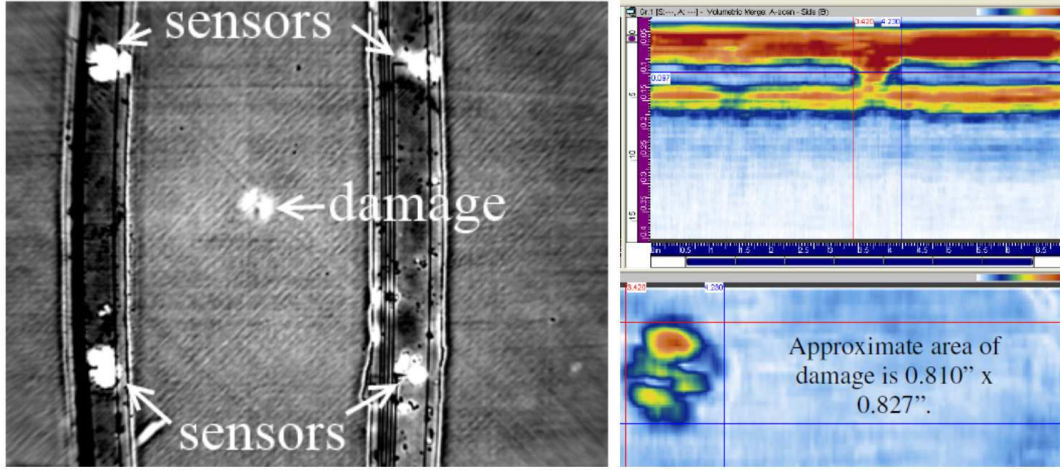


Figure 2: Shearography image (left) and ultrasonic image (right) of the damaged area near the mid-point of a unit cell of the sensor network.

hidden delaminations at the lower energy levels, barely visible (external) damage at intermediate levels, all the way up to visible damage at the higher energy levels. The structure of the impacted region is shown in Fig. 2.

A representative set of experimental signals are shown in Fig. 3 for two different carrier frequencies ($f_0 = 50$ and 90 kHz). The baseline measurements (in red) were collected before the panel was damaged. In order to highlight the effect of the fault, the corresponding baseline measurements are subtracted from damaged measurements, leaving the difference signals (in blue). One actuator–sensor pair exhibits the scattering by the fault (Fig. 3a), while data from the other pair are representative of the extinction (absorption + scattering) (Fig. 3b). The scattered (difference) signal shows appreciable time delay, as would be expected from the increased propagation distance (by a factor of $\sqrt{2}$), while the negligible time delay in the extinction signal shows that the effect of the fault in the path is mainly one of absorption.

WAVE PROPAGATION MODEL

Mindlin plate theory offers a highly accurate model of wave propagation that is suitable for locating damage whose size is of the order of the plate thickness. In this approach, the displacement of a material point (x, y, z) is expressed in terms of the vertical displacement $w(x, y, t)$ and two angles of rotation $[\Omega_x \ \Omega_y]^T \equiv \mathbf{\Omega}(x, y, t)$ about the surface normal at time t . Assuming each layer to be linear, isotropic, homogeneous, of infinite lateral extent, and of common Poisson ratio ν , and denoting the external load by $p(x, y, t)$, w and $\mathbf{\Omega}$ are found to obey the coupled equations [4, 5]

$$\frac{D}{2} [(1 - \nu)\nabla^2 \mathbf{\Omega} + (1 + \nu)\nabla\nabla \cdot \mathbf{\Omega}] - G(\mathbf{\Omega} + \nabla w) = I \frac{\partial^2 \mathbf{\Omega}}{\partial t^2}, \quad (2)$$

$$G(\nabla^2 w + \nabla \cdot \mathbf{\Omega}) + p = \rho \frac{\partial^2 w}{\partial t^2}. \quad (3)$$

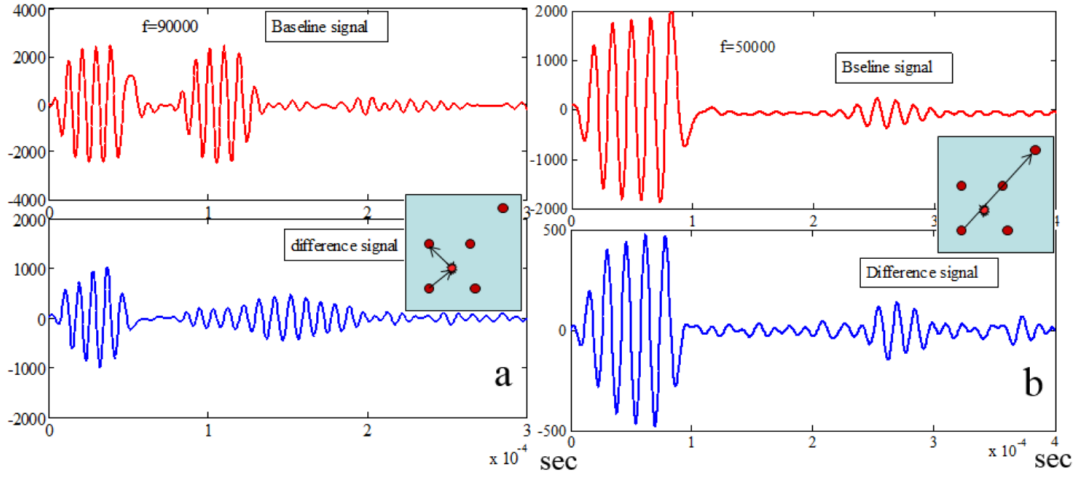


Figure 3: Baseline and difference signals for two actuator–sensor pairs, quantifying the degree of scattering (a) and extinction (b) by the fault. The large initial wave packet present in all the traces is a crosstalk signal (the “main bang”), which is windowed out for subsequent data processing.

Here, the effective flexural and shear stiffnesses D , G and vertical and rotary inertia ρ , I for the three-layer panel are calculated by averaging through the thickness of the layered structure [1], obtaining

$$\begin{aligned}
 D &= E_f t_f^3/6 + E_c t_c^3/12 + E_f t_f(t_f + t_c)^2/2, \\
 G &= \mu_c(t_c + t_f)^2/t_c, \\
 \rho &= 2\rho_f t_f + \rho_c t_c, \\
 I &= \rho_f t_f^3/6 + \rho_c t_c^3/12 + \rho_f t_f(t_c + t_f)^2/2,
 \end{aligned}$$

where subscripts c and f refer to the core and the face sheets, and E , μ , and t denote Young and shear moduli and layer thickness, respectively, with the total panel thickness being $h = 2t_f + t_c$.

Solutions of (2) and (3) have been detailed elsewhere [4, 5]; for the present purposes, the main result of interest are the wave numbers

$$k_{1,2} = \frac{\omega}{\sqrt{2}} \sqrt{\frac{I}{D} + \frac{\rho}{G} \pm \sqrt{\left(\frac{I}{D} - \frac{\rho}{G}\right)^2 + \frac{4}{\omega^2} \frac{\rho}{D}}}, \quad k_3 = \sqrt{\frac{2(I\omega^2 - G)}{D(1 - \nu)}}, \quad (4)$$

and the fact that k_2 and k_3 are cut off below $\omega_c = \sqrt{G/I}$.

Finally, scattering from a fault (e.g., a delamination) may be treated in two different ways. For barely visible faults, it is sufficient to treat the fault as a small local perturbation of the panel parameters, and employ the Born approximation for deriving the scattered waves. For more severe damage, the fault may be treated as an inhomogeneity with a simple shape (e.g., a cylinder), and solutions to (2) and (3) in the two different regions may be matched at the fault boundary.

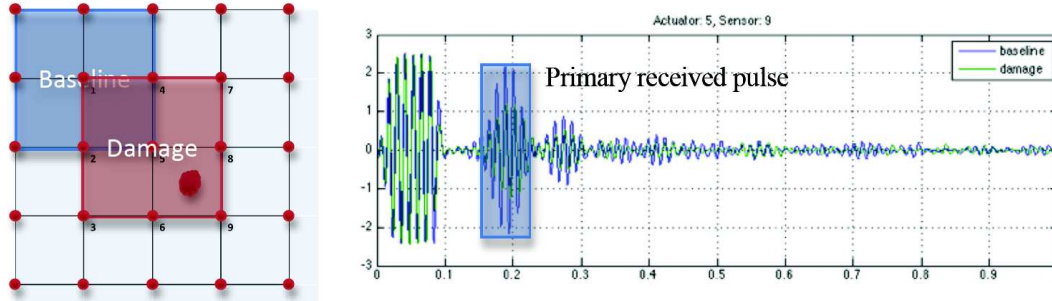


Figure 4: (Left) Baseline and damage surface areas used in the experiment. (Right) Comparison of acoustic wave packets transmitted across baseline and damaged paths.

INFERENCE PROBLEM

Tomographic fault detection

A scalable fault detection and localization algorithm was developed and tested using measurements collected from the experimental setup discussed above. Since this work was performed after the panel had been damaged, a spatially equivalent surface area was used to represent the baseline case (see Fig. 4). The tomographic fault detection approach presented in this section is motivated by the clear reduction in signal energy between the measured baseline and damage scenarios, as can be observed in Fig. 4.

We begin by overlaying an $n \times n$ grid on the surface area of interest, as shown in Fig. 5, where each cell in the grid is assigned an unknown coefficient of absorbed energy per unit length, denoted x_k for $k = 1, 2, \dots, n^2$, caused by possible damage in that cell. The net difference in transmitted signal energy between the baseline and the damage cases is then accounted for by writing

$$b_j = E_j^{\text{base}} - E_j^{\text{damage}} = \sum_{k \in I_j} a_{kj} x_k, \quad (5)$$

where j represents the path corresponding to a particular actuator–sensor pair, I_j represents the set of indices on the j -th path, and a_{kj} represents the length of the portion of the j -th path passing through the k -th cell. With m distinct paths, this leads to a set of m equations in n^2 variables, which we represent by the matrix–vector equation

$$Ax = b. \quad (6)$$

Generally, this system of equations will be underdetermined in x . One can, however, find meaningful candidate fault scenarios by looking for sparse solutions that closely satisfy this system of equations. (Because of measurement noise, one does not usually require the linear system to be satisfied exactly). Finding the sparsest solution to a set of linear equations is known to be a difficult combinatorial optimization problem; a heuristic method that tends to work well in applications is to solve the convex optimization problem

$$\text{minimize } \|Ax - b\|_2^2 + \lambda \|x\|_1, \quad (7)$$

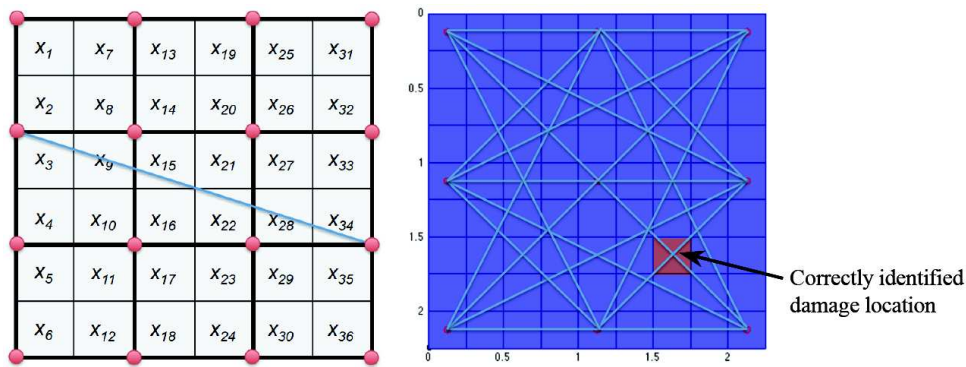


Figure 5: (Left) Notional sensor configuration and surface grid for tomographic damage detection technique. (Right) The actual surface grid, sensor configuration, and actuator-sensor paths for the experimental setup considered in this paper.

where λ is an algorithm tuning parameter, and $\|x\|_1$ denotes the ℓ_1 -norm defined as the sum of the absolute values of the elements of x [6–9].

As a proof of concept, this method was demonstrated using the same composite sandwich panel and experimental setup discussed above. Because much of the received acoustic signal contains spurious signal variation, a single pulse model for the primary pulse highlighted in Fig. 4 was fit using a standard nonlinear-least-squares approach. The normalized signal energy computed from the model fit for both baseline and damage cases was then used to determine the energy loss vector b . This was accomplished for each of the 81 paths in the 3×3 sensor network shown in Fig. 5. Using an existing numerical solver from [10] with $\lambda = 2$, we were able to recover a sparse representation, with a single non-zero element, correctly identifying the damage location on the panel (compare Figs. 4 and 5) in 92 ms on a standard PC.

Although further study of this heuristic approach is needed, the initial results show that it is capable of providing coarse fault location estimates without the need to directly infer sensitive time-of-flight related parameters (e.g., parameters governing the anisotropic velocity of propagation in the honeycomb structure). This approach scales well with increasing grid size n , which affords greater resolution in damage location. Furthermore, this algorithm can provide a quick, high-quality initial guess required by more quantitative approaches for fault detection and localization, such as the one considered next.

Model-based inference

A more quantitative approach to damage detection and localization, based on an underlying physics model, was undertaken next. This approach relies on a simple model of signal propagation in the panel, and solves for the unknown fault parameters via nonlinear least squares.

In order to isolate the signal due to damage, baseline measurements were subtracted from those obtained after the panel was damaged. Time-series data

were obtained by sampling this difference signal at the m -th sensor at time instants $t_n = t_0 + n\tau$, $n = 1, \dots, N$, where t_0 is a suitable time delay and τ is the sampling period. Assuming additive sensor noise, the model for the data is

$$z_m(n) = s_m(n) + \nu_m(n), \quad (8)$$

where $\nu_m(n)$ are uncorrelated Gaussian random variables with mean zero and variance σ^2 , and

$$s_m(n) = \alpha \frac{v(t_n - \|\boldsymbol{\rho}_m - \boldsymbol{\rho}_f\|/c - \|\boldsymbol{\rho}_f - \boldsymbol{\rho}_a\|/c)}{\|\boldsymbol{\rho}_m - \boldsymbol{\rho}_f\|}. \quad (9)$$

Here, α is an overall scale parameter that includes the scattering cross-section of the fault as well as the actuator and sensor gains, $v(t)$ is the Hann excitation signal given in (1), $\boldsymbol{\rho}_a$, $\boldsymbol{\rho}_m$, and $\boldsymbol{\rho}_f$ are two-dimensional vectors indicating the positions of the actuator, the m -th sensor, and the fault, respectively, and $c = \partial\omega/\partial k_1|_{\omega_0}$ denotes the group velocity of the wave packet; see (4). The model (9) thus assumes that dispersion is negligible, that the sensors are in the far field of the actuator, and that only the A_0 Lamb mode is propagating on the panel.

The determination of the unknown fault parameter vector $\boldsymbol{\theta} \equiv [\alpha \ \boldsymbol{\rho}_f]^T$ starts with the specification of a cost function \mathcal{J} that attains its minimum for the actual fault parameter values, say, $\boldsymbol{\theta}^*$. A cost function based on measured and modeled signal energies was found to be robust in this regard [11]:

$$\mathcal{J}(\boldsymbol{\theta}) = \frac{1}{2} \sum_{m=1}^M (\mathcal{A}_m - \mathcal{E}_m)^2, \quad (10)$$

where M is the number of available sensor data streams, and

$$\mathcal{A}_m = \frac{1}{N} \sum_{n=1}^N [z_m(n)]^2 \quad \text{and} \quad \mathcal{E}_m = \frac{1}{N} \sum_{n=1}^N [s_m(n)]^2 + \sigma^2$$

are the time-averaged and ensemble-averaged signal energies, respectively. (Note that \mathcal{A}_m is computed from data while \mathcal{E}_m is based on the model developed above.) Initializing the search for fault parameters with a guess $\boldsymbol{\theta}_0$, the iteration

$$\boldsymbol{\theta}_{j+1} = \boldsymbol{\theta}_j - \lambda \nabla_{\boldsymbol{\theta}} \mathcal{J}(\boldsymbol{\theta}_j), \quad (11)$$

$j = 0, 1, \dots$, is carried out with a suitable learning parameter λ until the parameters converge to $\boldsymbol{\theta}^*$. Some typical inference results are shown in Fig. 6, with convergence achieved in only a few iterations of (11).

CONCLUSION

Two algorithms have been developed for detecting and localizing damage on composite sandwich panels. Both algorithms rely on nonlinear least squares estimation, even though they have distinctly different flavors in terms of the level of physics modeling incorporated into the inversion problem. A test panel consisting of an aluminum honeycomb and carbon-fiber face sheets was constructed, and a delamination fault was subsequently induced via a controlled impact. Both algorithms correctly localized this small (sub-inch) fault from experimental data, showing promise for further study in more realistic settings.

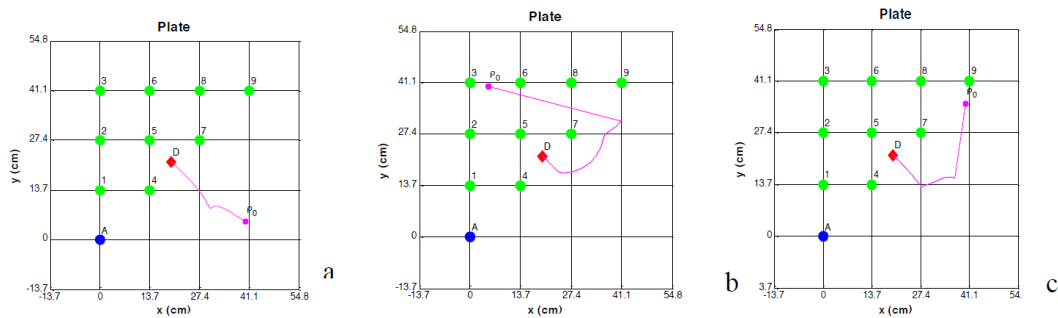


Figure 6: Grid of PZT transducers used for damage detection. The signal launched by the actuator (blue node) is picked up at various sensors (green nodes). Damage (red diamond) is correctly located from various initial guesses (magenta circles) via nonlinear least squares.

ACKNOWLEDGMENT

The authors would like to thank Shawn Beard and Howard Chung from Acellent Technologies, Inc., for their help in installing SMART Layer® sensors and for the opportunity to use their equipment.

REFERENCES

- [1] D. Zenkert, *An Introduction to Sandwich Structures*. EMAS Ltd. London, 1995.
- [2] B. Bednarczyk, S. Arnold, C. Collier, and P. Yarrington, “Preliminary structural sizing and alternative material trade study for CEV crew module,” in *48th AIAA/ASME/ASCE/AHS/ASC Structures, Structural Dynamics, and Materials Conference*, (Honolulu, HI), April 2007.
- [3] www.Acellent.com.
- [4] C. Vemula and A. Norris, “Flexural wave propagation and scattering on thin plates using Mindlin theory,” *Wave Motion*, vol. 26, pp. 1–12, 1997.
- [5] R. Rose and C. Wang, “Mindlin plate theory for damage detection: Source solutions,” *J. Acoust. Soc. Am.*, vol. 116, no. 1, pp. 154–171, 2004.
- [6] S. Boyd and L. Vandenberghe, *Convex Optimization*. Cambridge, UK: Cambridge University Press, 2004.
- [7] A. Ruszczyński, *Nonlinear Optimization*. Princeton, NJ: Princeton University Press, 2006.
- [8] S. Kim, “An interior-point method for large-scale ℓ_1 -regularized least squares,” *Journal of Machine Learning Research*, vol. 8, pp. 1519–1555, July 2007.
- [9] E. Candes, M. Wakin, and S. Boyd, “Enhancing sparsity by reweighted ℓ_1 minimization,” *Journal of Fourier Analysis and Applications*, vol. 14, pp. 877–905, December 2007.
- [10] K. Koh, S. Kim, and S. Boyd, “l1_ls: Simple matlab solver for ℓ_1 -regularized least squares problems (web page and software).” http://stanford.edu/~boyd/l1_ls, 2008.
- [11] L. Wang and F. Yuan, “Active damage localization technique based on energy propagation of Lamb waves,” *Smart Structures and Systems*, vol. 3, no. 2, pp. 201–217, 2007.